Dyes and Pigments 153 (2018) 182–188

Contents lists available at ScienceDirect

Dyes and Pigments

journal homepage: www.elsevier.com/locate/dyepig

Synthesis of novel light harvesters based on perylene imides linked to triphenylamines for Dyes Sensitized Solar Cells

Carlos Alberto Echeverry[a,b,c], Robert Cotta[b], Alberto Insuasty[c], Alejandro Ortíz[a], Nazario Martín[c], Luis Echegoyen[b], Braulio Insuasty[a,*]

[a] Departamento de Química, Facultad de Ciencias Naturales y Exactas, Universidad del Valle, A.A. 25360 Cali, Colombia
[b] Chemistry and Computer Science, University of Texas at El Paso, 79968-0519 El Paso, TX, United States
[c] Departamento de Química Orgánica, Facultad de Química, Universidad Complutense, 28040 Madrid, Spain

ARTICLE INFO

Keywords:
Dye-sensitized solar cells
Organic dyes
Perylene-based dyes
Electron transfer
Photovoltaic

ABSTRACT

Dye Sensitized Solar Cells (DSSCs) are promising optoelectronic devices that use renewable energy and organic or organometallic dyes as light harversters. They exhibit moderate overall efficiencies of power conversion that can be increased by improving the light-harvesting capacity of the organic dyes. Here, we report the synthesis, structural and electronic properties of two novel dyes based on perylene imides **PI-1** and **PI-2** as well as their application in DSSCs. In our design, design triphenylamine electron donors were linked to perylene-3,4,9,10-tetracarboxylic dianhydride derivative. The new dyes showed a broad absorption spectrum in the visible region as well as a strong *push – pull* electronic interaction determined computationally. Photovoltaic values for these dyes were not higher than previously reported compounds based on perylenes, with the best photovoltaic performance observed for the DSSCs based on **PI-2**, with an overall conversion efficiency of 1.3% under AM 1.5 irradiation (100 mW cm^{-2}). Although the electron transport to the TiO_2 surface for **PI-1** and **PI-2** was not efficient enough to result in a high photovoltaic behavior, our design has afforded dyes exhibiting a more efficient light capture in the visible region.

1. Introduction

Since the original work published by Grätzel and co-workers in 1991 [1], Dye-sensitized solar cells (DSSCs) have become an important topic of research, especially due to their promise as alternatives to conventional and more expensive photovoltaic devices based on silicon. In a typical DSSC device, light is absorbed by a monolayer of dye molecules which generally are organic compounds based on an electron donor moiety linked to an acceptor group that also functions as the anchor on the TiO_2 surface. When light is absorbed by the dyes, electrons are transferred from their Highest Occupied Molecular Orbital (HOMO) of the donor moiety to the Lowest Unoccupied Molecular Orbital (LUMO) of the acceptor group, and are injected into the conduction band of the TiO_2, thus generating an electric current [2,3].

One of the most important components of these cells is the organic dye, which need to meet certain requirements for an efficient electron transfer to the conduction band of the TiO_2 and hence result in efficient power conversion. These requirements are namely: (i) Dye should be a stable electron donor compound with a broad absorption spectrum absorbing light in the visible range; (ii) The oxidation potential of the donor moiety should be lower than the I^-/I_3 redox couple, ensuring an efficient dye regeneration as well as a stabilized charge-separated state; (iii) There must be a strong interaction between TiO_2 and the LUMO level localized near the anchoring group of the dye, ensuring good electronic coupling [4,5]. In addition, it is worth noting that the reduction potential of dyes should be higher than the conduction band level of the TiO_2 to ensure an efficient electron injection.

Several electron-donors have been used in DSSCs, such as porphyrins [6,7], *ex*TTF [8,9] and triphenylamines (TPA) [10–14], to name a few, the latter has been used in the design of many dyes exhibiting high efficiencies. On the other hand, the use of electron-acceptor groups as anchoring units to the TiO_2 have been limited to cyanoacrylic acid and 3-acetic-rhodanine acid, the former exhibiting better performance because it preserves the conjugation of the system with lower charge recombination rates and relatively high injection charge density into the TiO_2 electrode when compared with 3-acetic-rhodanine acid [15–17]. Recently, we reported the synthesis of 2-(1,1-dicyanomethylene)rhodanine (DCR) as an anchoring unit without the –COOH group, which showed a moderate conversion efficiency when it was linked to TPA units [18].

* Corresponding author.
E-mail address: braulio.insuasty@correounivalle.edu.co (B. Insuasty).

https://doi.org/10.1016/j.dyepig.2018.02.009
Received 10 November 2017; Received in revised form 1 February 2018; Accepted 4 February 2018
Available online 06 February 2018
0143-7208/

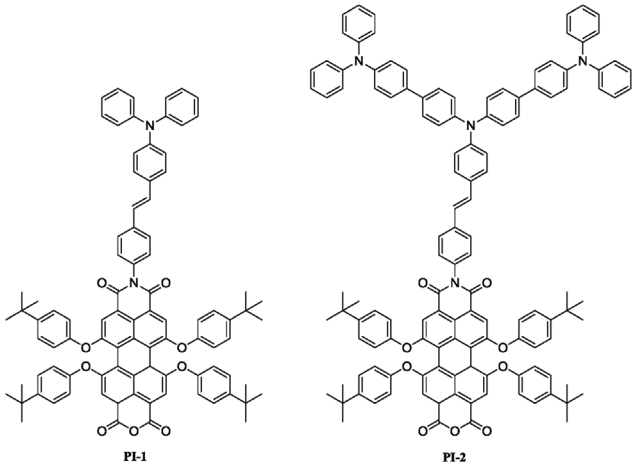

Fig. 1. Molecular structure of dyes **PI-1** and **PI-2**.

Although, several organic dyes with promising results for DSSCs have been studied, there is still a need to design novel compounds with high light-harvesting abilities in the visible spectrum to improve the current densities of the devices [3]. For this reason, the use of perylene tetracarboxylic (mono- and bis-) imides (PIs) in optoelectronic devices has increased in the last decades [19], not only because of their strong absorption properties in the visible region with high molar extinction coefficients (ε = 30,000–90,000 l mol^{-1} cm^{-1}) but also due to their high photo-stability and electron-drawing ability [20,21]. Unfortunately, PIs show low solubility and high tendency to form π-π aggregates that could favor charge recombination reactions and hence limiting their applications in DSSCs devices. Therefore, the design of complex synthetic strategies to endow PIs units with functional groups that ensure solubility but also avoid π-π aggregation are required [22,23].

Taking this into account, herein, we report the synthesis and electronic characterization of two novel organic dyes based on perylene imides (PIs) (Fig. 1), which have been linked to TPA moieties. Perylene units were functionalized with *p-tert*-butylphenol moieties to improve their solubility, reduce a possible aggregation and increase their absorption in the visible region. As anchoring unit to the surface of TiO_2, the free dicarboxylic acid anhydride group in the perylene units is employed [24]. The introduction of PIs allows us to broaden the range of absorption of the new dyes and to evaluate the influence of π-conjugation on electron transfer.

2. Results and discussion

2.1. Synthesis of perylene monoimide dyes

The synthetic routes of all intermediate compounds and the target dyes are depicted in Schemes 1–3. In our design, the first hurdle was the low solubility of the perylene derivatives, which was overcome by substitution of the bay region of the perylene dianhydride with *p-tert*-butylphenol, leading to compound **5** in moderate yield. Subsequently, we synthesized the electron-donor compounds starting from phosphonates **6a-b** which via Horner-Emmons reactions gave rise to intermediates **7a-b**. Then, the reduction reaction of **7a** using hydrazine hydrate catalyzed by Raney nickel led to compound **8**. In the case of compound **10**, the same synthetic route was followed, but performing a Suzuki coupling of **7b** before the reduction reaction. The target dyes (**PI-1** and **PI-2**) were synthesized following literature procedures [25], showing an enhanced solubility in solvents such as dichloromethane, chloroform and tetrahydrofuran. All compounds were characterized using ^{1}H and ^{13}C NMR, as well as mass spectrometry. The ^{1}H NMR spectrum of dye **PI-1** showed a singlet around 8.26 ppm corresponding to the aromatic protons of the perylene, and two doublets around 7.62 and 7.42 ppm corresponding to the protons of the phenyl ring bound directly to the perylene moiety by means of an amide group. The strong signals observed at the high field, around 1.33 and 1.29 ppm, correspond to the 36 methyl protons of the *tert*-butyl groups. In addition, ^{13}C NMR presented 34 signals clearly showing carbonyl carbon resonances of the carboxamide ring around 163.5 and 160.0, as well as the carbon signals of the *tert*-butyl groups at high field. The ^{1}H and ^{13}C NMR spectra were similar for dye **PI-2** (see Fig. S1 and S2, supplementary Information).

2.2. Absorption and emission properties

The absorption spectra of **PI-1** and **PI-2** in different solvents ($CHCl_3$ and THF) and emission spectra in chloroform are shown in Fig. 2. Spectra are compared with the solar spectral irradiance AM 1.5 and data are summarized in Table 1. Spectroscopic characteristics of the new dyes show typical features of perylene-based compounds, showing two absorption bands around 455 nm and 580 nm, corresponding to a $\pi-\pi^*$ transition and charge transfer band, respectively [26].

A hypsochromic shift can be observed with an increase of the molar extinction coefficients when solvent polarity is changed from non-polar (chloroform, ε_T = 4.8) to a more polar aprotic solvent (tetrahydrofuran, ε_T = 7.5), which could be attributed to a solvent-induced change of the ground-state structure from a less dipolar to a strongly dipolar PI induced structure [27]. In the case of **PI-1**, it can be observed a broad single absorption band around 376 nm in THF that splits in two bands (350 and 390 nm) in chloroform, which could be attributed to a lower degree of aggregation of the **PI-1** in THF probably due to its higher solubility, leading to an increase in the absorbance [28]. It is also worth noting that the spectroscopic characteristics of **PI-2** remained unchanged when the conjugation was increased by addition of electron-donor units of TPA [29].

The absorption spectra for **PI-1** and **PI-2** were compared with the solar spectral irradiance AM 1.5 (Fig. 2a), showing that the introduction of perylene as a highly conjugated system broadened the absorption into the visible range with molar extinction coefficients for the lowest transition band around 50,000 M^{-1} cm^{-1}, which are similar to the previously described absorption coefficients reported for dyes based on perylene monoimides [19,21].

The emission spectra for **PI-1** and **PI-2** in chloroform showed a fluorescence emission maxima at an excitation wavelength of 586 nm and 588 nm, respectively (Fig. 2b). The fluorescence quantum yields (ϕ_F) were also measured in chloroform with an excitation wavelength of 557 nm using a comparative method (eq. (1)) [30,31]:

$$\phi_F = \phi_F^{std} \frac{IA^{std}\eta^2}{I^{std}A\eta_{std}^2} \quad (1)$$

Where I and I^{std} are the areas under the fluorescence curves of the dyes **PI-(1-2)** and standard, respectively. A and A^{std} are the respective absorbances of the sample and standard at the excitation wavelengths, and n^2 and n_{std}^2 are the refractive indices of solvents used for the sample and standard, respectively. Rhodamine B (RB) in EtOH (ϕ_F^{std} = 0.68) was employed as standard (see Fig. S3a, supplementary information).

The emission band structure for **PI-1** and **PI-2** was independent of the excitation wavelength. The maximum emission was similar for both dyes, however, the emission intensity for **PI-2** was ~three-fold larger than for **PI-1**, which could be attributed to the presence of the two additional units of TPA. It is also worth noting that the increase in the emission intensity leads to a fluorescence quenching for **PI-1** (ϕ_F = 0.012) in comparison to **PI-2** (ϕ_F = 0.029) (Table 1).

2.3. Electrochemical properties

Electrochemical potentials *vs* Fc/Fc$^+$ measured in anhydrous

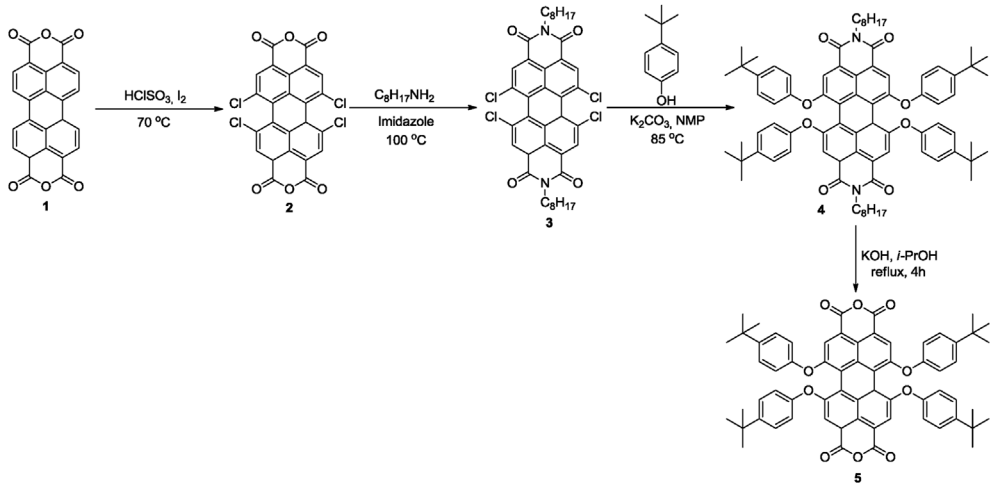

Scheme 1. Synthesis of perylene dianhydride derivate **5** as previously describe [25].

dichloromethane at a concentration of 0.5 mM are summarized in Table 2, using compound **4** as reference. The cyclic voltammetry of **4** showed two reversible reduction waves at −1.236 and −1.388 V and one reversible oxidation wave at +0.792 V, each of them corresponding to one-electron transfer process. All the synthesized dyes exhibited similar electrochemical behavior to that of compound **4**, exhibiting reversible redox waves. Both, **PI-1** and **PI-2**, showed two reversible reduction waves (Table 2), the first one being anodically shifted compared to **4**, indication of a better electron accepting ability due to the LUMO stabilization upon introduction of the dicarboximide with the TPA substituent [32]. The first oxidation potential at +0.392 V corresponds to the oxidation of the TPA, which was followed by the oxidation of the perylene which was anodically shifted approximately 110 V in comparison with compound **4** (Fig. 3a). In the case of **PI-2**, three oxidation processes corresponding to the oxidation of the donor system unit were observed (Fig. 3b), the first oxidation wave being cathodically shifted compared to **PI-1,** could be an indication of a better electron donor ability. These electrochemical results confirmed the *push-pull* features of **PI-(1-2)**, where TPA moieties were showed to be strong electro donor and PI was confirmed to be a good electron acceptor.

2.4. Theoretical calculations and solar cell performance

Density functional theory (DFT) calculations were used to understand the electronic structure of the synthesized dyes. Fig. 4a shows the structure of **PI-1** and **PI-2** optimized by B3LYP using the 6-31G (d, p) hybrid functional. In our design, the substitution of the bay region of the PI with *p-tert*-butylphenol and the use of bulky electron donor units as compound **10** could decrease the aromatic π-π stacking in the dyes as well as hinder the approach of the triiodide to the surface of the TiO_2 because of the orientation assumed by the phenyl rings in TPA donors, thus inhibiting charge recombination (see Fig. S4, supplementary information).

The lowest transition energies for the new dyes were calculated using the CAM-B3LYP functional with the CPCM model in chloroform as solvent, which shows that the HOMO orbital is localized mainly on the electron donor group while the LUMO orbital is localized on the perylene electron acceptor, showing a strong *push – pull* interaction between them (Fig. 4a). However, it is worth noting the presence of a nodal point on the topology of the frontier orbitals, exactly on the dicarboximide ring, which decreases the electronic interaction for the whole system (see Fig. 2a) [29].

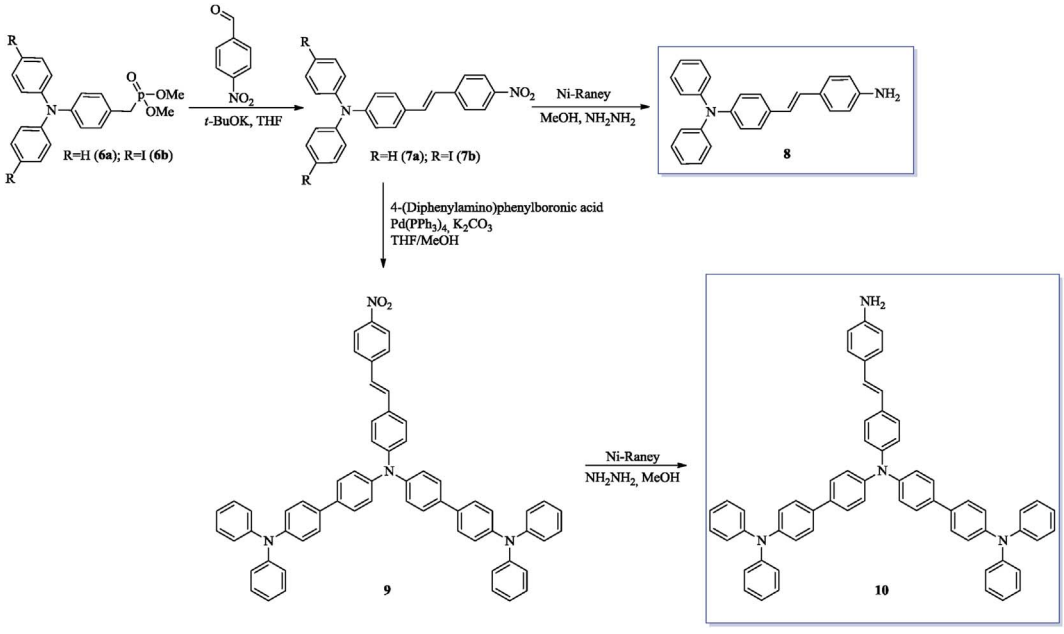

Scheme 2. Synthesis of TPA derivatives.

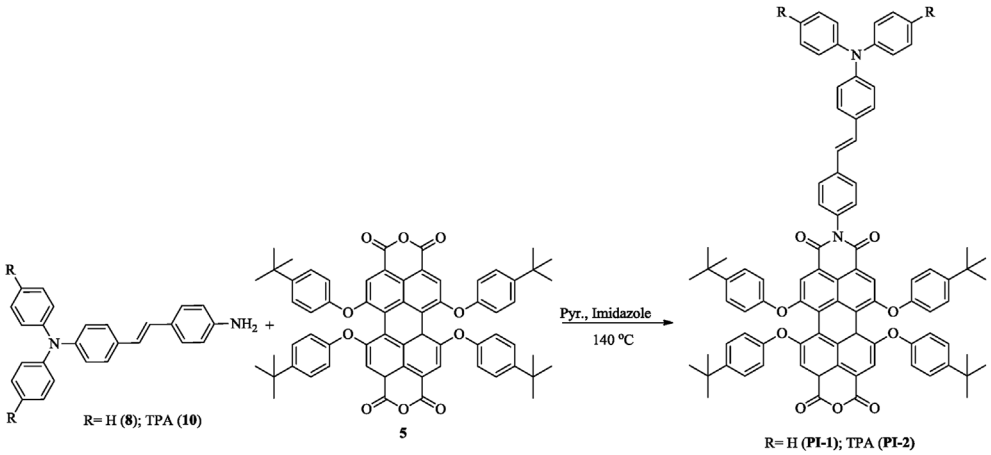

Scheme 3. Synthesis of PIs dyes.

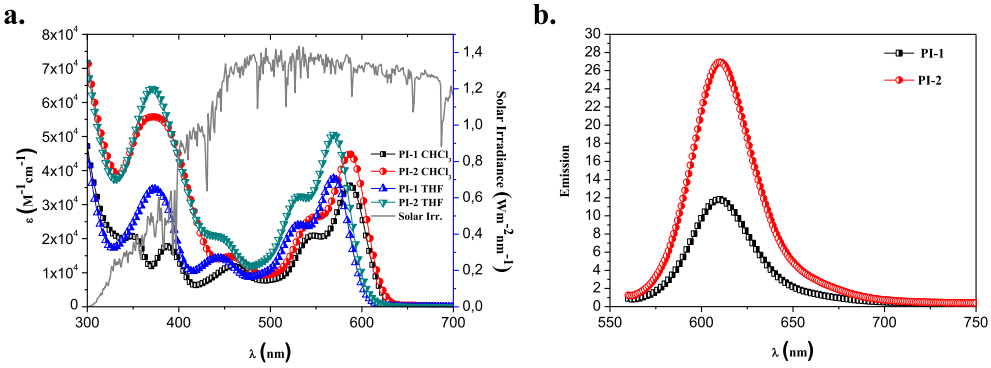

Fig. 2. Electronic spectra of **PI-1** and **PI-2** at a concentration of 1×10^{-5} M: **a.** Absorption in $CHCl_3$ and THF; **b.** Emission in $CHCl_3$.

Table 1
Photophysical properties of **PI-(1,2)**.

Dye	λ_{max}^{Abs}/nm [ε, $M^{-1}cm^{-1}$][a]		λ_{max}^{Em} [nm]	ϕ^{b}	E/eV [nm][c]	f^{c}
	$CHCl_3$	THF				
PI-1	586 (35,600)	569 (37,700)	1.03	0.012	2.28 (543)	0.7331
PI-2	588 (44,900)	570 (50,500)	0.62	0.029	2.33 (532)	1.0302

[a] λ_{max}^{Abs} corresponds to the maximum absorption in the visible range at a concentration of 1×10^{-5} M.
[b] Rhodamine B in EtOH ($\phi_F^{std} = 0.68$) was employed as standard [30]. All compounds were used at a concentration of 1×10^{-6} M.
[c] The excitation energy (E) and oscillator strength (*f*) were calculated using TD-DFT/CAM-B3LYP.

Table 2
Electrochemical potentials (V) *vs* Fc/Fc^+ of **PI-(1, 2)** and compound **4** as a reference.

Dye	E_{ox}^1	E_{ox}^2	E_{ox}^3	E_{ox}^4	E_{red}^1	E_{red}^2	E_g[a]
4	+0.792	–	–	–	−1.236	−1.388	2.031
PI-1	+0.392	+0.916	–	–	−1.052	−1.548	1.444
PI-2	+0.241	+0.450	+0.615	+0.904	−1.030	−1.187	1.271

[a] E_{gap} was determined by the equation $E_g = E_{onset\ ox} - E_{onset\ reducción}$.

As mentioned before, DSSC devices need to meet certain requirements for an efficient power conversion, when the HOMO – LUMO energy levels were compared with the energy requirements for DSSCs, we observed that the HOMO energy levels were lower than the I^-/I_3 redox couple (−4.90 eV vs vacuum), thus ensuring dye regeneration. However, although the dyes showed LUMO energies higher than the conduction band energy of the TiO_2 (−3.90 eV) with energy gap (E_{gap}) for **PI-1** and **PI-2** of 0.30 and 0.44 (Table 3, Fig. 4b), respectively, these were not far enough away to ensure an efficient electron injection to nanocrystalline TiO_2 film, leading to low photovoltaic parameters for devices made with these dyes.

Photovoltaic properties for the dyes are summarized in Table 3. The incident photo-conversion efficiency (IPCE) for the DSSCs based on **PI-1** and **PI-2** under an illumination of simulated solar radiation AM 1.5 at 100 mW cm^{-2} is showed in Fig. 4c. Photocurrent responses of the DSSCs based on **PI-2** were higher than that obtained with **PI-1**, which had an IPCE value higher than 21% in the range of 530–540 nm. However, although the effective light harvesting for both dyes (extended up to about 650 nm), the IPCE values were very low in this range because of poor photocurrent density (J_{sc}) generated for **PI-1** and **PI-2**, negatively influencing the overall efficiency (η%) for the DSSC devices (Table 3). The increase of 0.3% in the overall efficiency for **PI-2** compared with **PI-1** could be attributed to the stronger electron donating nature and the lower aggregation on TiO_2 due to the larger steric hindrance produced by the presence of the three TPAs.

3. Conclusions

Perylene dyes **PI-1** and **PI-2** were successfully synthesized in moderate yields. DSSC devices based on **PI-1** and **PI-2** showed low overall efficiencies of 1.0 and 1.3%, respectively, mainly owing to a weak driving force for the electron injection from the dyes to the conduction band of the TiO_2, leading to low photocurrent responses. However, although the use of perylene-based dyes led to low efficiencies, these were higher than 1.0%, not much different from other reported efficiencies for DSSCs using perylene dyes [26]. It is important to remark, however, the fact that the measured values are comparatively modest, they have been nicely rationalized which is a critical issue for further

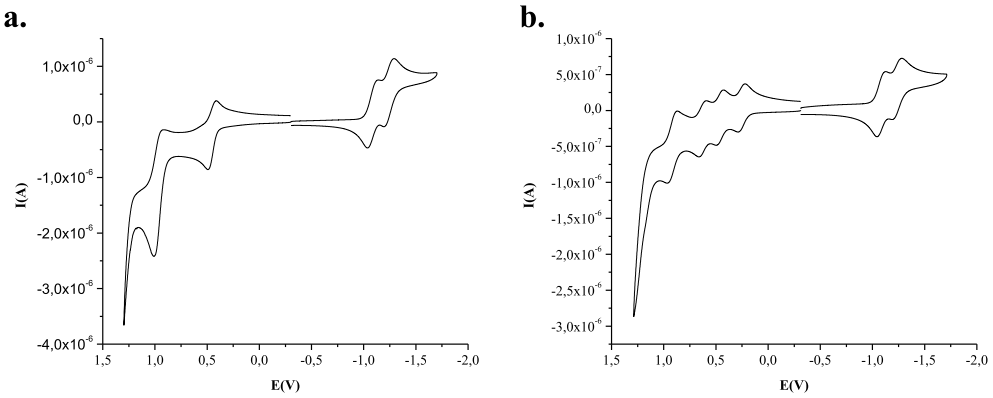

Fig. 3. Cyclic voltammograms for **a. PI-1** and **b. PI-2** in dichloromethane *vs* Fc/Fc^{+}.

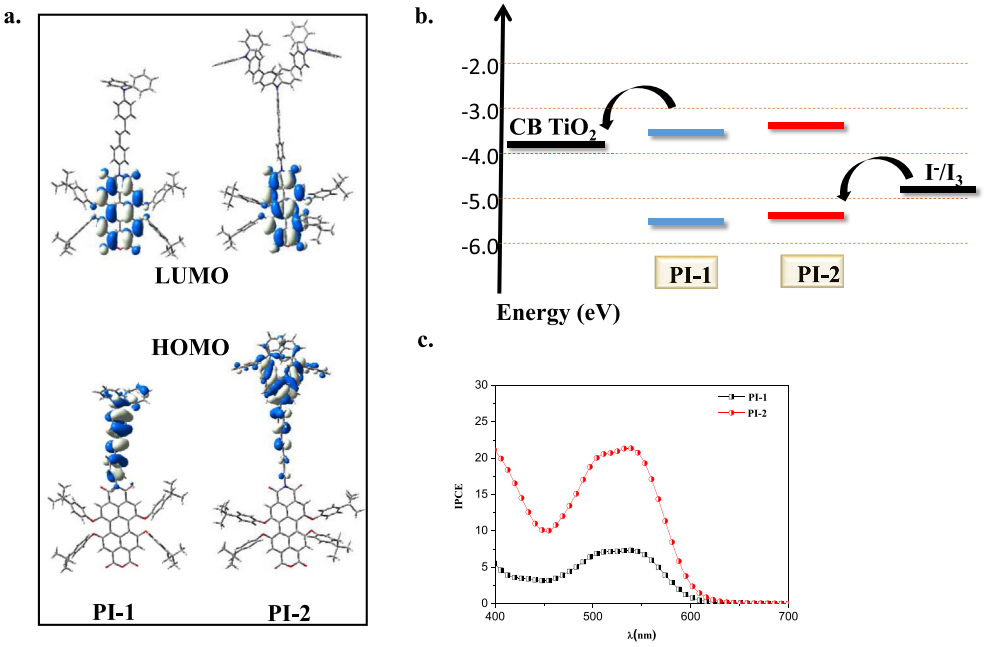

Fig. 4. Calculated and photovoltaic features for **PI-1** and **PI-2: a.** Frontier orbitals calculated using DFT with CAM-B3LYP/6-31G (d, p) functional; **b.** Energy requirements for DSSC devices; and **c.** IPCE spectra of the DSSC devices.

Table 3
Estimated energy levels for **PI-1** and **PI-2**.

Dye	$E_{ox\ vs\ NHE}$ [V][a]	E_{HOMO} [eV][b]	E_{LUMO} [eV] (Egap)[c]	J_{sc} [mA cm^{-2}]	V_{oc} [V]	*FF*	η%
PI-1	0.932	−5.68	−3.60 (0.30)	2.13	0.635	0.723	1.00
PI-2	0.781	−5.53	−3.46 (0.44)	2.89	0.638	0.689	1.30

[a] Potentials measured *vs* the (Fc/Fc^{+}) couple were converted to the Normal Hydrogen Electrode (NHE) by addition of +0.63 V [6].

[b] Calculated with the formula: $E_{HOMO} = -(E_{[ox\ vs\ NHE]} + 4.75)$eV [33].

[c] Calculated with the formula: $E_{LUMO} = E_{HOMO} + E_{0\text{-}0}$, $E_{0\text{-}0}$ was calculated from the intercept of the normalized absorption spectra and the emission spectra (λ_{int}): $E = 1240\ eV\ nm/\lambda_{int}$ (see Figure S3b, supplementary information). E_{gap} is the energy gap between the E_{LUMO} of dye and the conduction band of the TiO_2 (−3.90 eV).

improved designs in DSSCs.

4. Experimentals

4.1. Materials and equipments

All solvents were dried according to standard procedures. Reagents were used as purchased. All air-sensitive reactions were carried out under an argon atmosphere. Flash chromatography was performed using silica gel (Merck, Kieselgel 60, 230–240 mesh or Scharlau 60, 230–240 mesh). Analytical thin layer chromatography (TLC) was performed using aluminum coated Merck Kieselgel60 F254 plates. NMR spectra were recorded on a Bruker Avance 400 (^{1}H: 400 MHz; ^{13}C: 100 MHz) spectrometer at 298 K using partially deuterated solvents as internal standards. Coupling constants (*J*) are denoted in *Hz* and chemical shifts (*δ*) in ppm. Multiplicities are denoted as follows: *s* = singlet, *d* = doublet, *t* = triplet, *m* = multiplet, *br* = broad. FT-IR spectra were recorded on a Shimadzu FT-IR 8400 spectrometer. UV-Vis spectra were recorded using a Shimadzu 1700 spectrometer using choloroform and tetrahydrofuran as solvent. The mass spectra were obtained on a Matrix Assisted Laser Desorption Ionization (coupled to a Time-Of-Flight analyzer) MALDI-TOF HP1100MSD spectrometer and a

Bruker REFLEX spectrometer respectively. Cyclic voltammetry was performed using an AutolabPGStat 30. A glassy carbon working electrode (Metrohm 6.0804.010) was used after being polished with alumina (0.3 μm) for 1 min, and platinum wire was used as the counter electrode. A silver wire was used as a pseudo-reference electrode. Tetra-*n*-butylammoniumhexafluorophosphate ($TBAPF_6$) (0.1 M) was used as supporting electrolyte in dry dichlorometane as solvent. The samples were purged with argon prior to measurement. The scan rate was 100 mV/s. The device measurements were made using a Photo Emmision Tech Solar Simulator SS100 Solar Simulator CC3. Melting point was measured using a Büchi melting point apparatus at 670 mmHg and was uncorrected. Microanalyses were performed on a LECO CHNS-900 elemental analyzer and the values are within ± 0.4% of theoretical values.

4.2. Synthesis and characterization

4.2.1. Perylene dianhydride derivatives **1-5**

All perylene compounds shown in Scheme 1 were synthetized following previously described methodologies [18]. All compounds showed the same spectroscopic properties.

4.2.2. General synthesis of compounds **7a-b**

A solution of *t*BuOK (0.229 g, 2.04 mmol) in THF (10 mL) was slowly added to a mixture of phosphonate (**6a** or **6b**) (1.36 mmol), 4-nitrobenzaldehyde (0.171 g, 1.13 mmol) and THF (20 mL). The reaction mixture was heated at 61 °C for 5 h under an inert atmosphere. Then the reaction was quenched with water (20 mL) followed by organic extraction with CH_2Cl_2. The Organic phases were dried over Na_2SO_4 and then the solvent was removed by rotary evaporation. The crude product was purified by column chromatography on silica gel (dichlorometane/hexane 3/1). Compound **7a** and its reduction product (**8**) showed the same spectroscopic properties as previously published [24].

4.2.3. (E)-N,N-(4′-iodophenyl)-4-(nitrostyryl)aniline (**7b**)

Red solid (53%, 555 mg), m.p. 133–135 °C at 670 mmHg. FTIR (KBr, cm^{-1}) υ = 2978, 2924, 1578, 1524, 1334, 1239, 852, 704. ^{1}H NMR ($CDCl_3$, 400 MHz) δ. 8.24 (2H, d, J = 12.0 Hz), 7.63 (2H, d, J = 8.0 Hz), 7.59 (4H, d, J = 8.0 Hz), 7.46 (2H, d, J = 12.0 Hz), 7.23 (1H, d, J = 16.0 Hz), 7.09–7.04 (3H, m), 6.88 (4H, d, J = 8.0 Hz) ppm. ^{13}C NMR ($CDCl_3$, 100 MHz) δ: 147.3, 146.6, 144.0, 138.5, 132.5, 131.2, 130.1, 129.5, 128.2, 126.6, 126.4, 125.1, 124.2, 123.8 ppm. MALDI-TOF-MS *m/z*: [M] calcd. for $C_{26}H_{18}I_2N_2O_2$: 643.950; found: 643.757. Anal. calc. for $C_{26}H_{18}I_2N_2O_2$: C, 48.47; H, 2.82; N, 4.35. Found: C, 48.41; H, 2.82; N, 4.37.

4.2.4. (E)-N,N-(4′-(4″-diphenylaminophenyl)phenyl)-4-(nitrostyryl) aniline (**9**)

Compound **7b** (290 mg, 0.45 mmol), 4-(diphenylamino)boronic acid (289.14 mg, 0.99 mmol) and K_2CO_3 (155.5 mg, 1.1 mmol) were refluxed in a mixture of THF/MeOH (5/1) under an argon atmosphere. Then $Pd(PPh_3)_4$ (52 mg, 0.045 mmol) was added and the temperature was kept at 70 °C. The reaction was quenched with water followed by organic extraction with CH_2Cl_2. The Organic phases were dried over Na_2SO_4 and then the solvent was removed by rotary evaporation. The crude product was purified by column chromatography on silica gel (chloroform/Methanol 50/1). Red solid (65%, 255 mg), m.p. 125–127 °C at 670 mmHg. FTIR (KBr, cm^{-1}) υ = 3037, 2977, 1570, 1508, 1347, 829, 754. ^{1}H NMR (THF-d_8, 400 MHz) δ: 8.23 (2H, d, J = 8.0 Hz), 7.78 (2H, d, J = 8.0 Hz), 7.60–7.54 (9H, m), 7.45 (1H, d, J = 20.0 Hz), 7.30–7.26 (10H, m), 7.23 (4H, d, J = 8.0 Hz), 7.16 (2H, d, J = 8.0 Hz), 7.15–7.11 (12H, m), 7.04 (4H, m) ppm. ^{13}C NMR (THF-d_8, 100 MHz) δ: 148.1, 147.8, 147.0, 146.5, 146.1, 144.5, 135.8, 134.6, 132.7, 130.8, 129.1, 128.0, 127.3, 127.1, 126.5, 124.8, 124.4, 124.2, 123.8, 123.7, 123.0, 122.7 ppm. MALDI-TOF-MS *m/z*: [M] calcd. for $C_{62}H_{46}N_4O_2$: 878.362; found: 878.359. Anal. calc. for $C_{62}H_{46}N_4O_2$: C, 84.71; H, 5.27; N, 6.37. Found: C, 84.67; H, 5.25; N, 6.34.

4.2.5. (E)-N,N-(4′-(4″-diphenylaminophenyl)phenyl)-4-(aminostyryl) aniline (**10**)

Hydrazine (1.0 mL) was added to a solution of compound **9** (0.18 mmol) and Raney nickel (100 mg) in MeOH (50 mL). The reaction mixture was warmed for 2 h, then the Raney nickel was filtered and the product was obtained by evaporation-induced precipitation without further purification. Yellow solid (84%, 193 mg), m.p. 154–157 °C at 670 mmHg. FTIR (KBr, cm^{-1}) υ = 3451, 3366, 3032, 1622, 1496, 881, 755. ^{1}H NMR (CD_2Cl_2, 400 MHz) δ: 7.55–7.50 (8H, m), 7.44 (2H, d, J = 8.0 Hz), 7.35 (2H, d, J = 8.0 Hz), 7.33 (8H, m), 7.21 (4H, d, J = 8.0 Hz), 7.16–7.14 (14H, m), 7.07 (4H, m), 7.00 (1H, d, J = 16.0 Hz), 6.93 (1H, d, J = 16.0 Hz), 6.70 (2H, d, J = 8.0 Hz), 3.84 (2H, s) ppm. ^{13}C NMR (CD_2Cl_2, 100 MHz) δ: 147.7, 146.8, 146.5, 146.4, 146.3, 135.0, 134.6, 132.8, 129.2, 127.8, 127.5, 127.3, 127.3, 127.2, 126.9, 124.3, 124.3, 124.2, 124.1, 124.0, 122.9, 114.9 ppm. MALDI-TOF-MS *m/z*: [M] calcd. for $C_{62}H_{48}N_4$: 848.338; found: 848.136. Anal. calc. for $C_{62}H_{48}N_4$: C, 87.70; H, 5.70; N, 6.60. Found: C, 87.74; H, 5.75; N, 6.65.

4.2.6. General synthesis of target dyes **PI-1** and **PI-2**

A solution of **5** (0.20 mmol), imidazole (2.0 g, 29.4 mmol) and pyridine (15 mL) were refluxed under an argon atmosphere. Then the amine derivative **8** or **10** (2.04 mmol) in pyridine (5 mL) was slowly added to a solution during 1 h. Subsequently, acetic acid (100 mL) was added to the reaction mixture and the ensuing precipitate was filtered off. The crude product was purified by column chromatography on silica gel (dichlorometane/hexane 4/1).

4.2.6.1. PI-1. Violet solid (25%, 60 mg), m.p. > 350 °C at 670 mmHg. FTIR (KBr, cm^{-1}) υ = 3060, 1694, 1649, 1589, 1435, 1328, 1236, 960. Uv-vis λ_{max} (ε/$M^{-1}cm^{-1}$, THF): 569 (37,700), 530 (23,900), 375 (34,800) nm. ^{1}H NMR ($CDCl_3$, 400 MHz) δ: 8.26 (4H, s), 7.62 (2H, d, J = 9.0 Hz), 7.42 (2H, d, J = 9.0 Hz), 7.30–7.25 (12H, m), 7.23 (2H, d, J = 8.0 Hz), 7.13 (4H, d, J = 8.0 Hz), 7.09–7.02 (6H, m), 6.88–6.85 (8H, m), 1.33 (18H, s), 1.29 (18H, s) ppm. ^{13}C NMR ($CDCl_3$, 100 MHz) δ: 163.5, 160.0, 156.6, 156.0, 152.6, 147.8, 147.7, 147.5, 138.2, 133.7, 133.4, 133.1, 131.2, 129.3, 128.7, 127.5, 127.0, 126.9, 126.8, 126.1, 124.6, 123.5, 123.1, 122.1, 121.6, 120.1, 120.0, 119.4, 119.3, 118.1, 34.4, 34.4, 31.4, 31.4 ppm. MALDI-TOF-MS *m/z*: [M] calcd. for $C_{90}H_{76}N_2O_9$: 1330.571; found: 1330.711. Anal. calc. for $C_{90}H_{76}N_2O_9$: C, 81.18; H, 5.90; N, 2.10. Found: C, 81.14; H, 5.84; N, 2.07.

4.2.6.2. PI-2. Violet solid (14%, 50 mg), m.p. > 350 °C at 670 mmHg. FTIR (KBr, cm^{-1}) υ = 2953, 2922, 1689, 1649, 1586, 1444, 1336, 1249, 995. Uv-vis λ_{max} (ε/$M^{-1}cm^{-1}$, THF): 570 (50,500), 529 (31,900), 372 (64,000) nm. ^{1}H NMR ($CDCl_3$, 400 MHz) δ: 8.26 (2H, s), 8.26 (2H, s), 7.63 (2H, d, J = 8.0 Hz), 7.52–7.48 (8H, m), 7.45 (2H, d, J = 8.0 Hz), 7.31–7.25 (19H, m), 7.21 (4H, d, J = 8.0 Hz), 7.16–7.14 (13H, m), 7.10 (2H, d, J = 8.0 Hz), 7.07–7.03 (4H, m), 6.88–6.85 (8H, m), 1.33 (18H, s), 1.29 (18H, s) ppm. ^{13}C NMR ($CDCl_3$, 100 MHz) δ: 163.5, 160.0, 156.6, 156.0, 152.6, 147.8, 147.7, 146.9, 146.2, 138.2, 135.3, 134.6, 133.8, 133.5, 133.1, 131.4, 130.9, 129.3, 127.6, 127.4, 127.3, 127.1, 126.9, 126.8, 124.6, 124.4, 124.0, 123.8, 123.1, 122.9, 122.1, 121.6, 120.1, 119.4, 119.3, 118.1, 34.4, 34.4, 31.4, 31.4 ppm. MS (MALDI-TOF): MALDI-TOF-MS *m/z*: [M] calcd. for $C_{126}H_{104}N_4O_9$: 1816.780; found: 1816.023. Anal. calc. for $C_{126}H_{104}N_4O_9$: C, 83.23; H, 5.77; N, 3.08. Found: C, 83.27; H, 5.71; N, 3.10.

Acknowledgment

The authors gratefully acknowledge financial support from COLCIENCIAS (Grant number 110656933745), Universidad del Valle, the US NSF (Grants DMR-1205302, PREM program and CHE-1408865), the Robert A. Welch Foundation (Grant AH-0033, endowed chair) for

generous financial support. We also thank the Financial support from the European Research Council ERC-2012-ADG_20120216 (Chirallcarbon), MINECO of Spain (CTQ2011-24652) and CAM (grant number MADRISOLAR-2 S2009/PPQ-1533).

Appendix A. Supplementary data

Supplementary data related to this article can be found at http://dx.doi.org/10.1016/j.dyepig.2018.02.009.

References

[1] O'regan B, Grätzel M. A low-cost, high-efficiency solar cell based on dye-sensitized colloidal TiO_2 films. Nature 1991;353(6346):737–40.
[2] Clarke TM, Durrant JR. Charge photogeneration in organic solar cells. Chem Rev 2010;110(11):6736–67.
[3] Hagfeldt A, Boschloo G, Sun L, Kloo L, Pettersson H. Dye-sensitized solar cells. Chem Rev 2010;110(11):6595–663.
[4] Wiberg J, Marinado T, Hagberg DP, Sun L, Hagfeldt A, Albinsson B. Effect of anchoring group on electron injection and recombination dynamics in organic dye-sensitized solar cells. J Phys Chem C 2009;113(9):3881–6.
[5] Jose R, Kumar A, Thavasi V, Fujihara K, Uchida S, Ramakrishna S. Relationship between the molecular orbital structure of the dyes and photocurrent density in the dye-sensitized solar cells. Appl Phys Lett 2008;93(2):023125.
[6] Yella A, Lee H-W, Tsao HN, Yi C, Chandiran AK, Nazeeruddin MK, et al. Porphyrin-sensitized solar cells with cobalt (II/III)–based redox electrolyte exceed 12 percent efficiency. Science 2011;334(6056):629–34.
[7] Hsieh C-P, Lu H-P, Chiu C-L, Lee C-W, Chuang S-H, Mai C-L, et al. Synthesis and characterization of porphyrin sensitizers with various electron-donating substituents for highly efficient dye-sensitized solar cells. J Mater Chem 2010;20(6):1127–34.
[8] Echeverry CA, Herranz MÁ, Ortiz A, Insuasty B, Martín N. Rhodanine-3-acetic acid and π-extended tetrathiafulvalene (exTTF) based systems for dye-sensitized solar cells. New J Chem 2014;38(12):5801–7.
[9] Wenger S, Bouit P-A, Chen Q, Teuscher J, Censo DD, Humphry-Baker R, et al. Efficient electron transfer and sensitizer regeneration in stable π-extended tetrathiafulvalene-sensitized solar cells. J Am Chem Soc 2010;132(14):5164–9.
[10] Echeverry CA, Cotta R, Castro E, Ortiz A, Echegoyen L, Insuasty B. New organic dyes with high IPCE values containing two triphenylamine units as co-donors for efficient dye-sensitized solar cells. RSC Adv 2015;5(75):60823–30.
[11] Tigreros A, Dhas V, Ortiz A, Insuasty B, Martín N, Echegoyen L. Influence of acetylene-linked π-spacers on triphenylamine–fluorene dye sensitized solar cells performance. Sol Energy Mater Sol Cells 2014;121:61–8.
[12] Pati PB, Yang W, Zade SS. New dyes for DSSC containing triphenylamine based extended donor: synthesis, photophysical properties and device performance. Spectrochim Acta Mol Biomol Spectrosc 2017;178:106–13.
[13] Qian X, Lan X, Yan R, He Y, Huang J, Hou L. T-shaped $(D)_2$–A–π–A type sensitizers incorporating indoloquinoxaline and triphenylamine for organic dye-sensitized solar cells. Electrochim Acta 2017;232:377–86.
[14] Caicedo M, Echeverry CA, Guimarães RR, Ortiz A, Araki K, Insuasty B. Microwave assisted synthesis of a series of charge-transfer photosensitizers having quinoxaline-2(1*H*)-one as anchoring group onto TiO_2 surface. J Mol Struct 2017;1133:384–91.
[15] Abbotto A, Manfredi N, Marinzi C, De Angelis F, Mosconi E, Yum J-H, et al. Di-branched di-anchoring organic dyes for dye-sensitized solar cells. Energy Environ Sci 2009;2(10):1094–101.
[16] Liu B, Li W, Wang B, Li X, Liu Q, Naruta Y, et al. Influence of different anchoring groups in indoline dyes for dye-sensitized solar cells: electron injection, impedance and charge recombination. J Power Sources 2013;234:139–46.
[17] Chen Y-C, Lin JT. Multi-anchored sensitizers for dye-sensitized solar cells. Sustain Energy Fuels 2017;1:969–85.
[18] Echeverry CA, Insuasty A, Herranz MÁ, Ortíz A, Cotta R, Dhas V, et al. Organic dyes containing 2-(1,1-dicyanomethylene)rhodanine as an efficient electron acceptor and anchoring unit for dye-sensitized solar cells. Dyes Pigments 2014;107:9–14.
[19] Li C, Wonneberger H. Perylene imides for organic photovoltaics: yesterday, today, and tomorrow. Adv Mater 2012;24(5):613–36.
[20] Langhals H, Obermeier A, Floredo Y, Zanelli A, Flamigni L. Light-driven charge separation in isoxazolidine–perylene bisimide dyads. Chem Eur J 2009;15(46):12733–44.
[21] Edvinsson T, Li C, Pschirer N, Schöneboom J, Eickemeyer F, Sens R, et al. Intramolecular charge-transfer tuning of perylenes: spectroscopic features and performance in dye-sensitized solar cells. J Phys Chem C 2007;111(42):15137–40.
[22] Chen Z, Stepanenko V, Dehm V, Prins P, Siebbeles LD, Seibt J, et al. Photoluminescence and conductivity of self-assembled π–π stacks of perylene bisimide dyes. Chem Eur J 2007;13(2):436–49.
[23] Zhang L, Cole JM. Dye aggregation in dye-sensitized solar cells. J Mater Chem A 2017;5(37):19541–59.
[24] Zhang L, Cole JM. Anchoring groups for dye-sensitized solar cells. ACS Appl Mater Interfaces 2015;7(6):3427–55.
[25] Panda DK, Goodson FS, Ray S, Lowell R, Saha S. Multichromophoric dye-sensitized solar cells based on supramolecular zinc-porphyrin⋯ perylene-imide dyads. Chem Commun 2012;48(70):8775–7.
[26] Shibano Y, Umeyama T, Matano Y, Imahori H. Electron-donating perylene tetracarboxylic acids for dye-sensitized solar cells. Org Lett 2007;9(10):1971–4.
[27] Homocianu M. Solvent effects on the electronic absorption and fluorescence spectra. J Adv Research Phys 2011;2(1):1–9.
[28] Block MAB, Hecht S. Poly(propylene oxide)−poly(phenylene ethynylene) block and graft copolymers. Macromolecules 2008;41(9):3219–27.
[29] Würthner F. Perylene bisimide dyes as versatile building blocks for functional supramolecular architectures. Chem Commun 2004:1564–79. 0.
[30] Magde D, Brannon JH, Cremers TL, Olmsted J. Absolute luminescence yield of cresyl violet. A standard for the red. J Phys Chem 1979;83(6):696–9.
[31] Williams ATR, Winfield SA, Miller JN. Relative fluorescence quantum yields using a computer-controlled luminescence spectrometer. Analyst 1983;108(1290):1067–71.
[32] Lee SK, Zu Y, Herrmann A, Geerts Y, Müllen K, Bard AJ. Electrochemistry, spectroscopy and electrogenerated chemiluminescence of perylene, terrylene, and quaterrylene diimides in aprotic solution. J Am Chem Soc 1999;121(14):3513–20.
[33] Cardona CM, Li W, Kaifer AE, Stockdale D, Bazan GC. Electrochemical considerations for determining absolute frontier orbital energy levels of conjugated polymers for solar cell applications. Adv Mater 2011;23(20):2367–71.